sciendo
Polish Journal of Medical Physics and Engineering
The Journal of Polish Society of Medical Physics
ISSN 1898-0309, doi: 10.2478/pjmpe-2019-0002
March 2019
Vol 25, Issue 1

Scientific Paper

GATE Simulation Study of the Siemens Biograph mCT 20 Excel PET/CT System

Rahal SAAIDI[1,a], Yassine TOUFIQUE[1,2], Abdelkrim ZEGHARI[1], Abderrahman EL KHARRIM[3], Rajaâ CHERKAOUI EL MOURSLI[1]

[1]*Faculty of Sciences, Mohammed V University, 4 Avenue Ibn Battouta B.P. 1014 RP, Rabat, Morocco*
[2]*Texas AM University at Qatar, Education City, Doha, Qatar*
[3]*Abdelmalek Essaadi University, Tetouan, Morocco*
[a]*E-mail address: saaidirahal@gmail.com*

(received 27 August 2018; revised 9 January 2019; accepted 15 January 2019)

Abstract

We used GATE simulation to study the effect of the coincidence time window (CTW) along with the block gap and the intercrystal gap on the count rate performance and the spatial resolution of the Biograph™ mCT 20 Excel. We ran simulations on our local cluster to reduce computation time. The task was split into several jobs that were then triggered simultaneously on the cluster nodes. The Biograph™ mCT 20 Excel was validated using the NEMA NU 2-2012 protocol. Our results showed good agreement with experimental data. The simulated sensitivity, peak true count rate, peak noise equivalent count rate (NECR), and scatter fraction showed agreement within 3.62%, 5.77%, 0.6%, and 2.69%, respectively. In addition, the spatial resolution agreed within <0.51 mm. The results showed that a decrease in the coincidence time window and the block gap and an increase in the intercrystal gap increase the count rate performance and improve the spatial resolution. The results also showed that decreasing the coincidence time window increased the NECR by 27.37%. Changing the intercrystal gap from 0 to 0.2 mm and the block gap and from 4 to 0.4 mm increased the NECR by 5.53% and improved the spatial resolution at 1 cm by 2.91 % and that at 10 cm by 3.85%. The coincidence time window, crystal gap, and block gap are important parameters with respect to improving the spatial resolution.

Key words: PET; NEMA; scatter fraction; sensitivity; NECR; spatial resolution.

Introduction

Positron emission tomography (PET) is a medical imaging technique used to diagnose cancer based on the three-dimensional (3D) distribution of a radiotracer in the target organ. PET is based on coincidence detection of two 511-keV photons produced by an electron-positron annihilation and emitted in opposite directions [1,2], taking into account the applied coincidence time windows (CTW), and dead time module to a specific volume. The CTW is defined as the maximum time period within which two single events are considered as a coincidence event by the coincidence sorter module of the PET acquisition system [3].

Modern PET scanners are coupled with computed tomography (CT) systems for more precise anatomical localization of cancer [4]. The combined PET/CT system – considered a major development in nuclear medicine – creates complex corrected PET images by multiplying the emission scan by the attenuation correction map generated by X-ray CT. This enhances count rate and spatial resolution and upgrades clinical conditions, diagnostics, development, and treatment planning [4].

In order to manufacture new scanners, it is necessary to optimize the acquisition protocols and ameliorate the scanner performances. Knowing that the scanner performance is affected by its design and the scintillating material [5]. The increase of the true coincidence counts related to the prompt counts that can improve the statistical quality of the acquired projection data and minimize the noise impact, consequently this improvement is the main objectives of a PET acquisition protocol optimization studies [6-8]. In addition, the statistical quality of the acquired projection data does not only depend on the acquisition protocol, but also on the other parameters as the properties of patients and scanner [3,7,9]. Certain studies about scanner technical parameters has been performed, such as the energy window, the coincidences time window, the dead time, and the detectors type, covering most of the configurations currently applied in recent clinical PET scanners [3,8-10].

The scan time and the initial amount of administered activity into the patient are the most important acquisition protocol parameters affecting statistical quality of the acquired projection data [3].

The administered activity (dose A_{adm}) depends on the intensity of activity distribution A_t at time t. It's related with the NECR by a nonlinear curve with a peak at moderate dose levels. The NECR increases until it reaches a plateau peak by the increasing of administered activity for smaller amounts of A_{adm}, while for high activity, NECR decrease, because of the high random coincidence count rates and the same for dead-time and pile-up effects [3].

Monte Carlo techniques are very efficient tools for simulating stochastic processes involved in radiation detection [11]. Several Monte Carlo packages for designing complex configurations are available (e.g., PENELOPE, MCNP, GEANT4, EGSnrc) [11].

The free open-source software GATE is frequently used for simulating tomographic experiments for PET and single-photon emission CT (SPECT) systems because of its flexibility [12]. GATE includes specific modules required to perform realistic simulations of nuclear medicine experiments. These modules allow easy control of the most important parameters on which the precision of the Monte Carlo simulation depends, including the description of the detector geometry, the description of the source geometry, and the acquisition process. The user builds the geometry and activates a model of physics process needed for the simulation by executing a simple configuration file (a macro file) containing commands interpreted by GATE [13].

The GATE simulations can be used to enhance imaging systems that help identify diseases earlier, provide accurate disease characterization, and improve therapy planning and monitoring. However, the simulations require important computing resources.

The research presented here focused on the Siemens Biograph™ mCT 20 Excel PET/CT scanner (Siemens Healthcare GmbH, Erlangen, Germany). we addressed the validation of GATE V7.1 simulations according to the NEMA (National Electrical Manufacturers Association) NU 2-2012 protocol [14,15] and compared the results to the experimental data. we know that the CTW and scanner design are two parameters which affect the NECR. The NECR increase by decreasing the CTW and choose the best scanner design [8,10]. Taking into account the relation between patient size over scanner FOV diameter and CTW. We studied the effect of the CTW and the block gap and intercrystal gap on the count rate and spatial resolution in order to optimize the A_{adm} to the patient using the Siemens Biograph^{TM} mCT 20 Excel scanner.

Methods and materials

In this section, the model (i.e., the geometry, physics, and signal processing), the computing grid and simulation, and the measurement protocols are described.

Table 1 Characteristics of the clinical PET/CT BiographTM mCT 20 Excel.

Detector material	LSO
Crystal dimensions (mm^3)	4 × 4 × 20
Detector ring diameter (cm)	84.2
Detector elements per block	169
Blocks per detector ring	48
Detector total number	24,336
Axial field of view (mm)	164

Model

The characteristics, including geometry, of the Biograph mCT 20 Excel PET/CT scanner used in this work are summarized in **Table 1**. The GATE code makes it easy to generate geometrically complex structures using combinations of simple shapes (e.g., boxes, spheres, and cylinders, as defined in GEANT4). Other necessary parameters are also considered in the simulation, including the physics process of photon interaction, for which we used the standard Rayleigh, photoelectric, and Compton energy models, with electron range = 30 mm, secondary electron = 1 GeV, and X-ray energy = 1 GeV; and the digital detection chain modeled using GATE to collect the data output.

The complete signal-processing chain was simulated using the adder module, readout module, crystal-blurring module, paralyzable or non-paralyzable dead-time module, energy-window module, and coincidence sorter module. The adder module generates a pulse from the energy deposited in each crystal, which the readout module processes to create a new pulse specific to the crystal block. Then, an energy resolution is applied in the crystal-blurring module, followed by application of the dead-time module and the energy-window module on the single-event level [12]. The preceding steps generate a single-event file containing a list of single events. Application of the coincidence sorter module to the single-event file creates the ROOT coincidence file, taking into account the coincidence pair events within the coincidence time window and the applied death time.

Job splitting and running the PET simulation on a local cluster

In general, Monte Carlo simulations are highly suited for parallelization and show a theoretical linear increase in processing speed as a function of the number of processing nodes. To reduce the overall computation time of the GATE simulations, we performed parallel execution of the simulations on a local cluster, which was managed by the open-source package TORQUE version 6.1.0 based on the original wrapper PBS [16,17] and comprised 12 nodes, each with a dual-core Intel Xeon 3-GHz processor (Intel Corp., Santa Clara, CA, USA) and 8 GB of memory.

The simulation runs comprised three steps: job splitting (preprocessing), the actual simulations, and file merging (post-processing). To reduce the computation time of a complete PET experiment simulation, a "job splitter" divided the task into several jobs. If the exponential radioactive decay of the used radioisotope is considered, the acquisition time decomposition approach to dividing the task involves dividing the experiment into a number of smaller experiments of equal length. Time-domain decomposition based on equal time intervals is inefficient. Each time interval defines a partial simulation of the whole experiment and is associated with a single job to be submitted to the Grid. A realistic PET experiment simulation task is divided into several smaller simulation jobs that run simultaneously on the Grid. Each job is run on GATE with an initial activity and partial acquisition time in such a way that the outputs obtained from each job are merged. The size of the output data can vary from a few megabytes to several gigabytes, depending on the parameters used for the simulation, particularly the acquisition time and activity concentration. The stored output data (i.e., ROOT files) contain coincidence events; detailed information on the energy deposited, the position of annihilation, and the coordinates of detection within the modeled scanner geometry; the number of Compton interactions that occurred while tracking each photon; and the eventID.

The ROOT files from the parallel simulations are the input that is merged to obtain the output file. The information of the split file, generated by the job splitter, is used to merge the ROOT files into a single output file. Finally, because the eventIDs are not the same as that of a single CPU simulation, the last eventID of each subsimulation is used as an offset for the next subsimulation. The output data are transferred from the local cluster to the local storage disk of the user interface computer and merged into a single file using the corrected eventIDs. The ROOT platform is then used to access the data for analysis.

NEMA protocol

Scanner sensitivity represents the efficiency of photon annihilation detection and is expressed as the detected coincidence event rate measured in counts per second (cps) per MBq [1,15]. This parameter was measured using the NEMA NU 2-2012 sensitivity phantom that comprises five concentric 70-cm-long aluminum tubes placed around the line source, which consists of a plastic tube containing the radioisotope ^{18}F. The latter tube had an inner diameter of 2 mm and the outermost tube had a diameter of 3.0 mm. The used radioactivity was sufficiently low such that the count losses and random events were negligible, with the single-event count losses and the random event rate at <5% and <1% of the true rate, respectively. The sensitivity was calculated with the phantom [14,15] placed at two positions: in the center of the scanner and 10 cm from the center of the field of view (FOV) of the scanner.

The scatter fraction (SF) and the noise equivalent count rate (NECR) were measured using the NEMA NU 2-2001 phantom. This phantom is a cylindrical 70-cm-long tube with an outer diameter of 20.3 cm. It is made of polyethylene with the required density of 0.96 g/cm. The ^{18}F was inserted into the plexiglass line source tube, which had an outer diameter of 5 mm and an inner diameter of 3 mm, and was positioned inside a 6.4-mm-diameter hole at the offset distance of 4.5 cm from the central axis of the phantom [1,2,14].

The spatial resolution describes the degradation that occurs during the acquisition of the ^{18}F source point image and corresponds to the shortest distance between two point sources by which they are discernible on the acquired image. The spatial resolution factor was calculated using the NEMA NU 2-2012 protocol in the transverse slice radially, tangentially, and axially. The point source was placed at six different positions ((x = 0, y = 1, z = 0), (x = 0, y = 10, z = 0), (x = 10, y = 0, z = 0), (x = 0, y = 1, z = 3/8 of the axial FOV), (x = 0, y = 10, z = 3/8 of the axial FOV), and (x = 10, y = 0, z = 3/8 of the axial FOV) cm) [1,14,15]. The images used to calculate the spatial resolution were reconstructed using the Software for Tomographic Image Reconstruction (STIR) with Filtered Back Projection 3D Reprojection (FBP3DRP) algorithm [18]. In addition, C++ analysis code, developed by the openGATE collaboration [6], was used to build a sinogram by applying a Radon transformation to simulated data (ROOT format) and import it into STIR, where the reconstruction algorithm in FBP3DRP code was applied. The spatial resolution of the images was calculated with A Medical Imaging Data Examiner (AMIDE) [19] for each of the six different positions in the radial, tangential, and axial profiles using the full-width at half-maximum (FWHM) of the resulting point spread function.

Calculation methodology

The counting of true, scatter, and random coincidences is controlled by the definition of the parameter given by the user during data analysis. We defined true coincidence as two photons produced by the same annihilation that did not interact with the scatter phantom. Scatter coincidence occurs when one of the two photons interacts with the scatter phantom before reaching the detector. Random coincidence occurs when two photons originate from different annihilations.

For the GATE simulation of data analysis, we used a C++ program to calculate the number of true, scatter, and random coincidences based on a ROOT coincidence file. This file contained an array of multiple rows and columns, where each row corresponded to a specific ID coincidence and the columns contained the information of each photon, including the event ID number, the energy deposited, the detection coordinates, and the number of Compton and Rayleigh interactions. Those parameters were used to classify the coincidences as true, random, or scatter.

Figure 1 shows the flow chart of the program that counts true, random, and scatter coincidences, which are used to calculate the Sensitivity, SF, and NECR parameters.

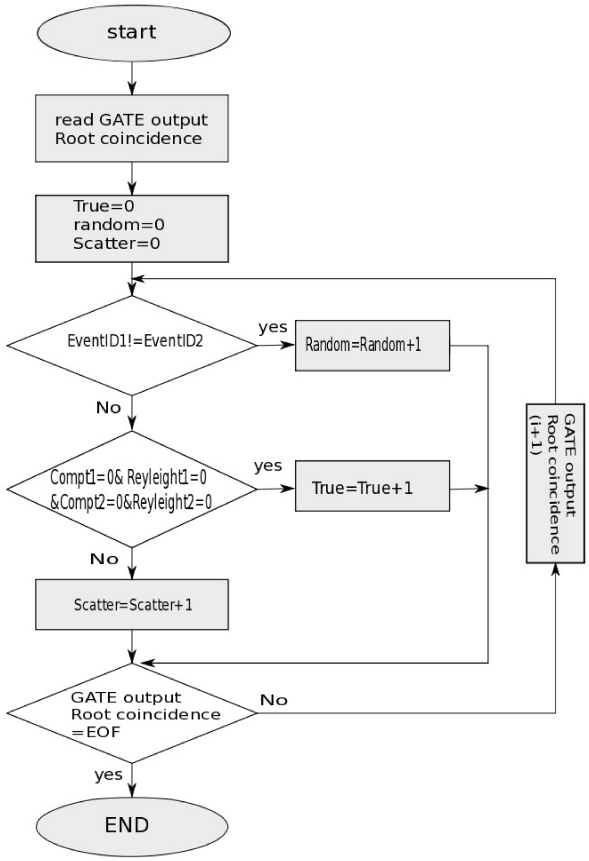

Figure 1. Flow chart for the C++ program that counts true, random, and scatter coincidences.

The sensitivity is defined by the following expression:

$$S=\frac{T}{A} \quad \text{Eq. 1}$$

where T is the count rate of the true coincidences and A is the activity of the source.

The SF parameter is calculated using the following expression:

$$SF=\frac{S_c}{S_c+T} \quad \text{Eq. 2}$$

where S_c and T are the simulated count rates of the scatter and true coincidences, respectively [2].

The NECR is calculated using the following expression:

$$NECR=\frac{T^2}{T+S_c+R} \quad \text{Eq. 3}$$

where R is the count rate of the random coincidences [7].

Results

In this section, the simulation results obtained for the performance parameters (SF, sensitivity, NECR), spatial resolution, and true count rates are described.

Figures 2 and **3** show the sensitivity of the detector for ^{18}F as count versus the thickness of aluminum in the phantom placed at the center and 10 cm from the center of the FOV of the scanner, respectively. The experimental data for sensitivity is compared with the simulation results (expressed in cps/kBq) in **Table 2** and the same comparison for the SF is given in **Table 3**.

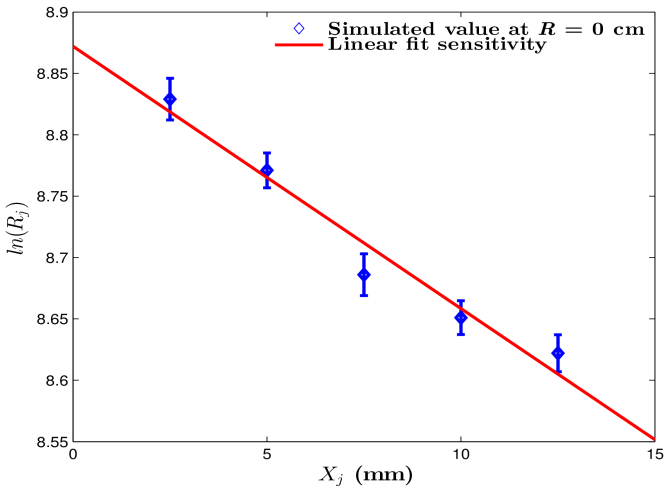

Figure 2. Sensitivity as a function of the shielding thickness of the phantom placed at the center of the FOV.

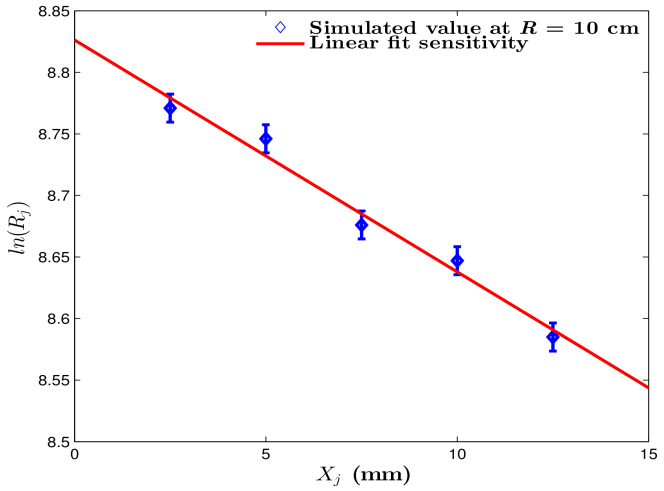

Figure 3. Sensitivity as a function of shielding thickness of the phantom placed 10 cm from the center of the FOV.

Table 2. Sensitivity parameter for the PET/CT Biograph™ mCT 20 Excel, calculated using the NEMA NU 2-2012 protocol [10].

Experimental results (cps/kBq)	5.8
Simulation results (cps/kBq)	6.01 ± 0.0021

Table 3. Scatter fraction (SF) parameter for the PET/CT Biograph™ mCT 20 Excel.

Experimental results	33 %
Simulation results	32.11 %

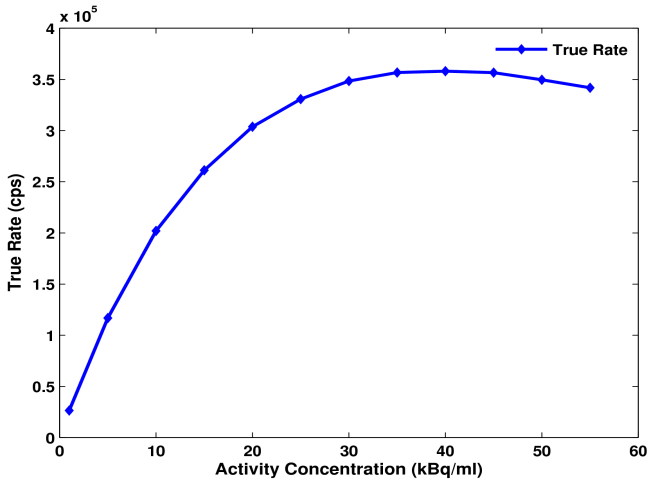

Figure 4. True count rate as a function of the source activity concentration.

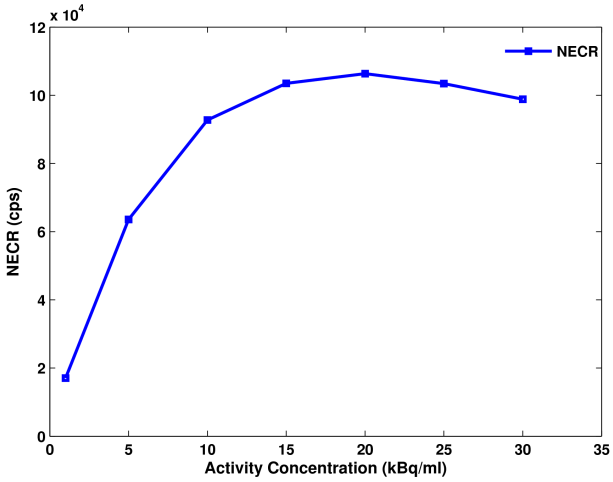

Figure 5. NECR as a function of the source activity concentration.

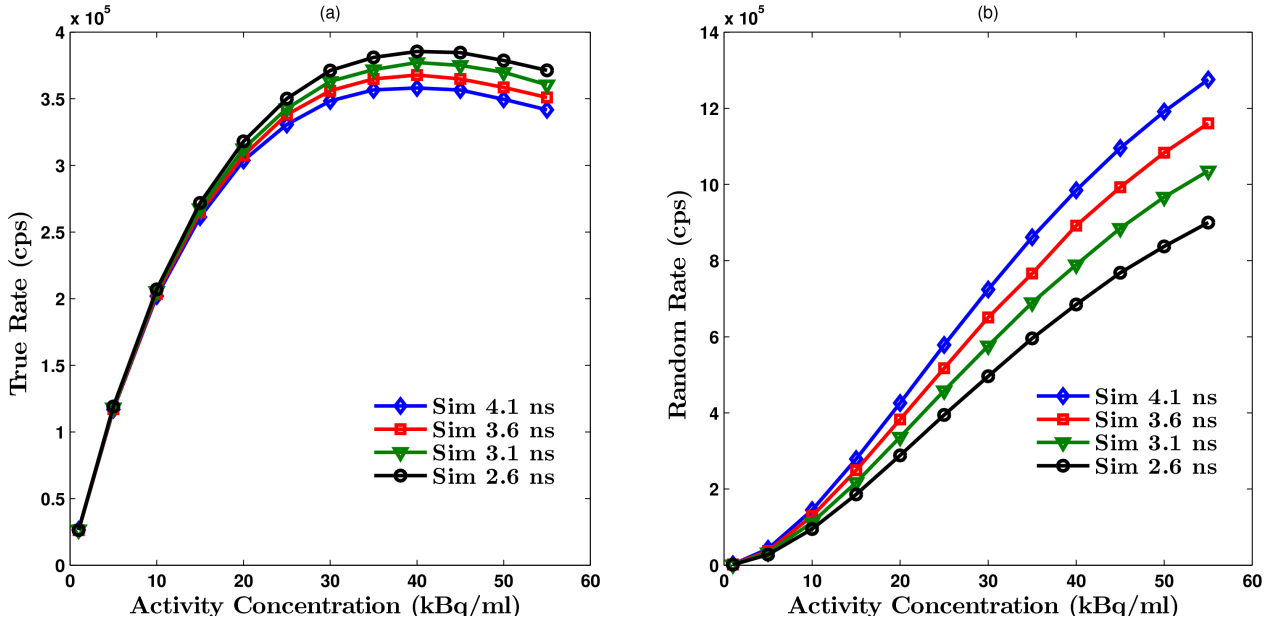

Figure 6. True rate vs. activity concentration for varying coincidence time windows.

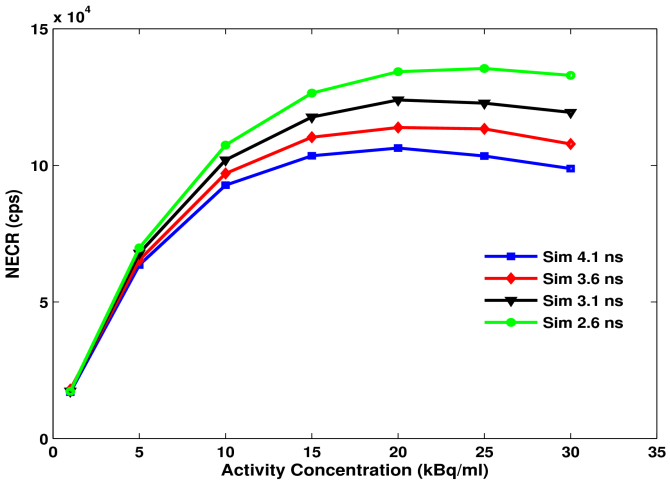

Figure 7. NECR vs. activity concentration for varying coincidence time windows.

Table 4. Peak true rate parameter for the PET/CT Biograph™ mCT 20 Excel.

Experimental results cps	380,000 @ ≤ 46 kBq/cm^3
Simulation results cps	358,070 @ 40 kBq/cm^3

Table 5. Noise equivalent count rate (NECR) peak for the PET/CT Biograph™ mCT 20 Excel.

Experimental results cps	107,000 @ ≤ 30 kBq/cm^3
Simulation results cps	106,349 @ 20 kBq/cm^3

Table 6. Spatial resolution for the PET/CT Biograph™ mCT 20 Excel, calculated using the NEMA NU 2-2012 protocol [10].

	Experimental data	Simulation
FWHM (mm) @ 1 cm, transverse	6	5.49 ± 0.021
FWHM (mm) @ 10 cm , transverse	6.3	5.96 ± 0.0113
FWHM (mm) @ 1 cm, axial	5.7	5.47 ± 0.014
FWHM (mm) @ 10 cm, axial	6.2	5.72 ± 0.022

Figure 4 displays the true count rate parameter obtained from the simulation as a function of the source activity concentration. **Table 4** compares the experimental data for the peak true rate with the simulation results.

Figure 5 shows the simulation results for the NECR as a function of the source activity concentration. **Table 5** compares the experimental data for the NECR peak with the simulation results.

The simulated spatial resolution results are compared with the experimental data in **Table 6**.

Figure 6 shows the true count rates and the random rate for different coincidence time windows (4.1, 3.6, 3.1, and 2.6 ns) as a function of the source activity concentration, and **Figure 7** shows the NECR as a function of the source activity concentration.

Figures 8 and **9** show the true count rate and the NECR, respectively, as functions of the source activity concentration for different crystal gap/block gap combinations (0/4 mm, 0.1/2.2 mm, and 0.2/0.4 mm), and **Tables 7** and **8** summarize the peak true rate and the NECR peak for the same gap combinations.

Table 9 gives the transverse and axial spatial resolution at 1 and 10 cm for different crystal gap/block gap combinations (0/4 mm, 0.1/2.2 mm, and 0.2/0.4 mm), while **Table 10** presents the NECR peak for two detector models for several coincidence time windows and crystal gap/block gap combinations of 0/4 mm and 0.1/2 mm.

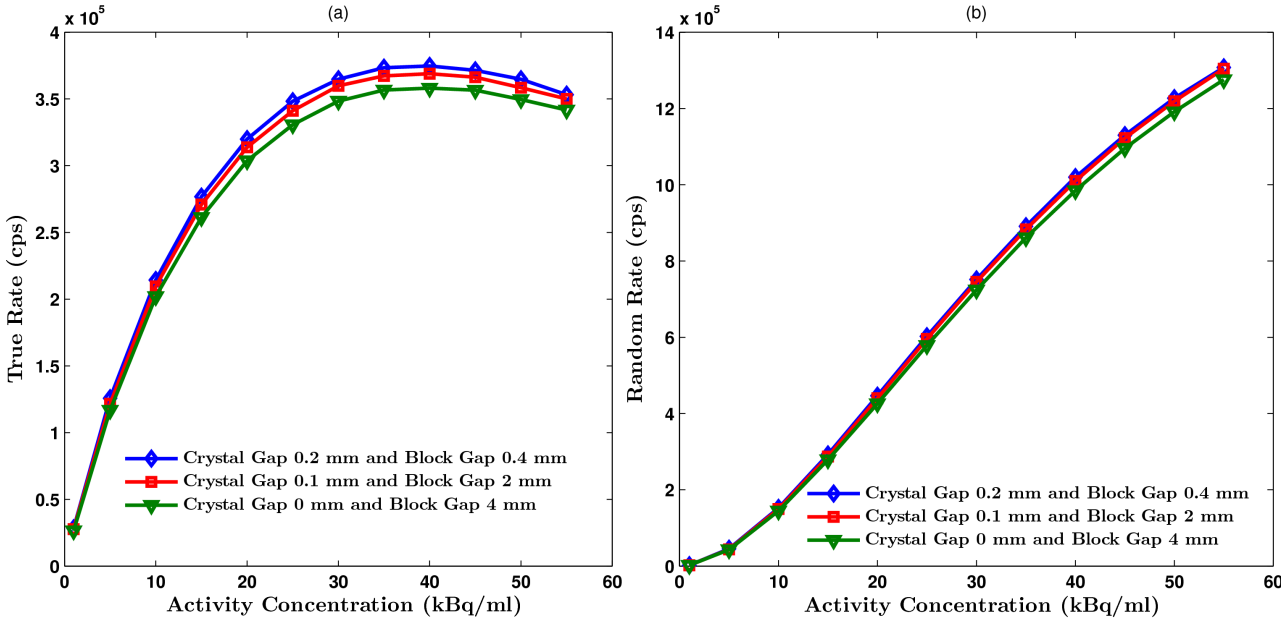

Figure 8. True rate vs. activity concentration for different crystal gap/block gap combinations.

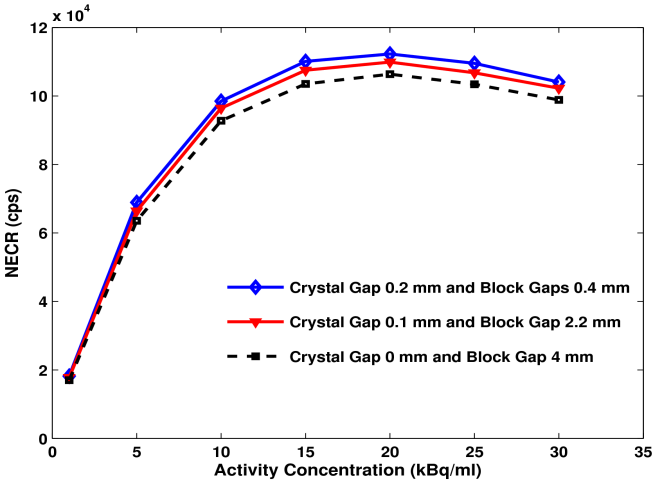

Figure 9. NECR vs. activity concentration for different crystal gap/block gap combinations.

Table 7. Peak true rate (cps) for different crystal and block gaps, calculated using the NEMA NU 2-2012 protocols [10].

0 mm crystal gap and 4 mm block gap	358,070 @ 40 kBq/cm^3
0.1 mm crystal gap and 2 mm block gap	368,968 @ 40 kBq/cm^3
0.2 mm crystal gap and 0.4 mm block gap	374,681 @ 40 kBq/cm^3

Table 8. Peak NECR (cps) for different crystal and block gaps, calculated using the NEMA NU 2-2012 protocol [10].

0 mm crystal gap and 4 mm block gap	106,349 @ 20 kBq/cm^3
0.1 mm crystal gap and 2 mm block gap	109,866 @ 20 kBq/cm^3
0.2 mm crystal gap and 0.4 mm block gap	112,234 @ 20 kBq/cm^3

Table 9. Spatial resolution for different crystal and block gap combinations, calculated using the NEMA NU 2-2012 protocol [10].

	No crystal gap and 4 mm block gap	0.1 mm crystal gap and 2 mm block gap	0.2 mm crystal gap and 0.4 mm block gap
FWHM (mm) @ 1 cm, trans.	5.49 ± 0.01	5.33 ± 0.003	5.24 ± 0.02
FWHM (mm) @ 10 cm, trans.	5.96 ± 0.01	5.73 ± 0.06	5.68 ± 0.06
FWHM (mm) @ 1 cm, axial	5.47 ± 0.01	5.44 ± 0.03	5.45 ± 0.01
FWHM (mm) @ 10 cm, axial	5.72 ± 0.02	5.62 ± 0.03	5.61 ± 0.007

Table 10. Peak NECR for two detector models with different coincidence time windows, calculated using the NEMA NU 2-2012 protocol [10].

	4.1 ns	3.6 ns	3.1 ns	2.6 ns
0 mm crystal gap and 4 mm block gap	106,349 @ 20 kBq/cm^3	113,851 @ 20 kBq/cm^3	123,916 @ 20 kBq/cm^3	135,462 @ 25 kBq/cm^3
0.1 mm crystal gap and 2 mm block gap	109,866 @ 20 kBq/cm^3	118,419 @ 20 kBq/cm^3	128,837 @ 20 kBq/cm^3	140,195 @ 25 kBq/cm^3

Discussion

In this section, we compare the simulation results with the experimental data from the data sheet for the Biograph^{TM} mCT 20 Excel obtained from Siemens.

The simulated sensitivity, reported in **Table 2**, agreed with the experimental data by 3.62%. The difference in the values is explained by the limitations of the photomultiplier tube (PMT) resolution and by the absence of the modeling of light shielding between the detector blocks in the GATE simulation [2].

The simulated SF parameter, reported in **Table 3**, agreed with the experimental data by 2.69%. The simulated peak true rate, reported in **Table 4**, agreed with the experimental data by about 5.77%. The difference is mainly due to the simple dead time model used in the simulation.

Table 5 presents the NECR peak value obtained from **Figure 5** and the experimental value. These values agreed within 0.6%, with the difference mainly due to the simple dead time model used in the simulation. The spatial resolution parameter of the simulated system, reported in **Table 6**, agreed with the experimental data within 0.51 mm.

Figure 6a shows that varying the coincidence time window did not affect the true coincidence rate at lower activity concentrations. However, at higher activity concentrations, the true rate increased slightly for shorter coincidence time windows (peak true rate increased by 7.66%). Moreover, **Figure 6b** shows that at the higher activity, the random rate has been decreased by a factor of 30 % for the smaller CTW.

Figure 7 shows significant improvement of NECR. This improvement is mainly due to the increase in the recorded true events and the decrease in the recorded random events for shorter coincidence time windows [13]. Using the smaller coincidence time window, the peak NECR increased by 27.37% when we change the simulated coincidence time window from 4.1 to 2.6 ns. The results suggest that a larger CTW induces a lower NECR and the smaller CTW induces a higher NECR. The relation between the NECR administered activity (dose A_{adm}) is a nonlinear curve with a peak at moderate dose levels. Moreover, the administered activity (dose A_{adm}) depend on the intensity of activity distribution A_t at time t, and the Administered dose is optimized when the NECR is maximized [3].

The larger CTW is also associated with smaller optimal doses while the smaller CTW increases the optimal dose. In addition, the decreasing of CTW decrease the FOV [10]. Therefore, the optimization of dose needs the use of specific CTW for A precise patient size. from our results the CTWs of 2.6, 3.1, 3.6, 4.1 ns are suggested to be used for the patient-size diameter (P_{size}) $\leqslant$ 40 cm , 40 cm $\leqslant P_{size} \leqslant$ 50 cm , 50 cm $\leqslant P_{size} \leqslant$56 cm and 56 cm $\leqslant P_{size}$ respectively.

Figure 8 shows that varying the crystal gap and the block gap did not affect the true coincidence rate at lower activity concentrations. However, at higher activity concentrations, the true rate increased slightly following an increase in the crystal gap and a decrease in the block gap. **Table 7** presents the peak true rate for different crystal gap and block gap values. The peak true rate increased by 4.63% when the crystal gap and block gap changed from 0/4 mm to 0.2/0.4 mm.

Figure 9 shows that varying the crystal gap and the block gap did not affect the NECR at lower activity concentrations. However, at higher activity concentrations, the NECR increased slightly following an increase in the crystal gap and a decrease in the block gap. This improvement is obtained by minimizing the penetration of the photons into the neighboring crystal, which minimizes the parallax effect [20]. The peak NECR, reported in **Table 8**, increased by 5.53% when the crystal gap/block gap changed from 0/4 mm to 0.2/0.4 mm.

The data in **Table 9** show that the transverse spatial resolution at 1 and 10 cm improved by 2.91% and 3.85%, respectively, and the axial spatial resolution at 1 and 10 cm improved by 0.5% and 1.74%, respectively, when the crystal gap/block gap combination changed from 0/4 mm to 0.1/2 mm. Moreover, the transverse spatial resolution at 1 and 10 cm improved by 1.68% and 0.8%, respectively, when the crystal gap/block gap changed from 0.1/2 mm to 0.2/0.4 mm. However, the axial spatial resolution at 10 cm improved by 0.177% and at 1 cm there was no improvement when the crystal gap/block gap changed from 0.1/2 mm to 0.2/0.4 mm. Hence, we conclude that the best model has a 0.1-mm crystal gap and a 2-mm block gap.

Table 10 presents the peak NECR for two detector models with crystal gap/block gap values of 0/4 mm and 0.1/2 mm and several coincidence time windows. The NECR of the model

with crystal gap/block gap values of 0.1/2 mm was better than that of the model with a crystal gap/block gap values of 0/4 mm.

Conclusion

The validation of the clinical Biograph mCT 20 Excel scanner using GATE V7.1 and the NEMA NU 2-2012 protocol showed that there was good agreement between the simulated and the experimental data for the scatter fraction, sensitivity, and count rate performance measurements and the spatial resolution. The results showed that the true coincidences and NECR increase when the coincidence time window is minimized, the crystal gap is increased, and the block gap is decreased.

The increase of NECR can improve the image quality and optimize the administered activity. to optimize the administered activity we suggest to use a specific CTW based on the patient size. However, the model with a 0.1-mm crystal gap and a 2-mm block gap showed improved spatial resolution.

Acknowledgements

The authors thank Mr. Andreas Dippold of Siemens Healthcare GmbH, Imaging & Therapy Systems, Molecular Imaging Europe, for providing the geometry and the data sheet of the scanner used in this study.

References

[1] Karakatsanis N, Sakellios N, Tsantilas NX, *et al*. Comparative evaluation of two commercial PET scanners, ECAT EXACT HR+ and Biograph 2, using GATE. Nucl Instrum Methods Phys Res A. 2006;569: 368-372.

[2] Toufique Y, Kaci M, El Kharrim A, *et al*. Grid Applied to Monte-Carlo Simulations of Positron Emission Tomography Systems. In: IBERGRID 2012 - 6th Iberian Grid Infrastructure Conference proceedings. 2012;123-133.

[3] Karakatsanis N, Loudos G, Rahmim A, Nikita KS. Monte-Carlo Based Characterization of the Counting Rate (NECR) Response for Personalized Optimization of the Administered Activity in Clinical PET Imaging. Frontiers Biomed Technol. 2014;1:14-34.

[4] Townsend DW. Physical Principles and Technology of Clinical PET Imaging. Ann Acad Med Singapore. 2004;33(2):133-145.

[5] Geramifar P, Ay MR, Shamsaie Zafarghandi M, *et al*. Performance Comparison of Four Commercial GE Discovery PET/CT Scanners: A Monte Carlo Study Using GATE. Iran J Nucl Med 2009;17(2):26-33.

[6] Karakatsanis N, Parasyris A, Loudos G, Nikita K. A Simulation study of the counting rate performance of clinical PET systems applying a methodology for optimizing the injected dose. IEEE Nucl Sci Symp Conf Record. 2008;5014-5019.

[7] Karakatsanis N, Nikita K. A simulation model of the counting rate response of clinical PET systems and its application to optimize the injected dose. IEEE Int Symposium on Biomedical Imaging: From Nano to Macro. 2009;398-401.

[8] Karakatsanis N, Loudos G, Nikita KS. A methodology for optimizing the acquisition time of a clinical PET scan using GATE. IEEE Nucl Sci Symp Med Imag Conf. 2009;2896-1901.

[9] MacDonald LR, Schmitz RE, Alessio AM, *et al*. Measured count-rate performance of the Discovery STE PET/CT scanner in 2D, 3D and partial collimation acquisition modes. Phys Med Biol. 2008;53(14):3723-3738.

[10] Geramifar P, Ay MR, Shamsaie Zafarghandi M, *et al*. Investigation of Time- of-Flight Benefits in an LYSO-Based PET/CT Scanner: A Monte Carlo Study Using GATE. Nucl Instrum Methods Phys Res A. 2011; 641;121-127.

[11] Nikolopoulos D, Kandarakis I, Tsantilas X, *et al*. Comparative Study of the Ra-diation Detection Efficiency of LSO, LuAP, GSO and YAP Scintillators for Use in Positron Emission Imaging (PET) via Monte-Carlo Methods. Nucl Instrum Methods Phys Res A. 2006;569:350-354.

[12] Gonias P, Bertsekas N, Karakatsanis NA, *et al*. Validation of a GATE Model for the Simulation of the Siemens PET/CT Biograph 6 Scanner. Nucl Instrum Methods Phys Res A. 2007;571:263-266.

[13] OpenGATE Collaboration: http://wiki.opengatecollaboration.org/index.php/Users_Guide_V7.1

[14] NEMA standards publication, NU 2-2012: Performance measurements of positron emission tomographs. Technical Report, National Electrical Manufacturers Association, Washington, DC, 2012.

[15] Rausch I, Cal-González J, Dapra D, *et al*. Performance evaluation of the Biograph mCT Flow PET/CT system according to the NEMA NU 2-2012 standard. EJNMMI Phys. 2015;2:1-17.

[16] http://www.adaptivecomputing.com/products/open-source/torque/

[17] De Beenhouwer J, Staelens S, Kruecker D, *et al*. Cluster computing software for GATE simulations. Med Phys. 2007;34(6):1926-33.

[18] Thielemans K, Tsoumpas Ch, Sauge D, *et al*. STIR Software for Tomographic Image Reconstruction: User's Guide, Version 3.0 , 2015, http://stir.sourceforge.net/documentation/STIR-UsersGuide.pdf.

[19] Loening A, Sau P. Amide a Medical Image Data Examiner: User's Manual V0.3.1, 2014, http://amide.sourceforge.net/help/C/index.html

[20] Lashkari S, Sarkar S, Ay MR, Rahmim A. The Influence of crystal Material on Intercrystal Scattering and the Parallax Effectin PET block Detectors: A Monte Carlo Study. In: Abu Osman NA, Ibrahim F, Wan Abas WAB, *et al*. (eds) 4th Kuala Lumpur International Conference on Biomedical Engineering 2008. IFMBE Proceedings, vol 21. Springer, Berlin, Heidelberg. p. 633-636.